4 Influence of Coupling in North Atlantic on Climate Variability

This chapter focuses on how air-sea interaction in the North Atlantic influences the local variability in the climate. This will be done by comparing two CCM1 climate simulations: a control simulation, whereby the SSTs are prescribed to follow the climatological annual cycle. and a coupled simulation in which the same model is coupled to the MLM of the North Atlantic. Standard statistical techniques are used to examine the climate of the coupled and the control simulations. The results presented in this chapter address how the natural variability of the model climate is changed by air-sea interaction.

The experiments and the data processing are described in Section 4-1. Impacts on climatology and variance are documented in Section 4-2. Correlations between air-sea variables are examined in Section 4-3. The natural patterns of variability in the coupled and control simulations are discussed in Section 4-4, and the discussion and a summary comprise the final two sections.

4.1 Experiment Setup and Model Data Processing

In the coupled (COU) simulation the MLM (see Section 1.3.1) is coupled to the NCAR CCM1 (see Section 1.3.2) between 20-60˚N (Figure 4-1) and is integrated beginning on the first of January for 35 1/3 years. The remaining ocean SSTs are specified according to the climatology of Alexander and Mobley (1976). The MLM is forced with heat, momentum,

and freshwater fluxes from CCM1 in the fully coupled method described in Figure2-1. Heat and salt flux corrections are added each day to the total heat and freshwater fluxes, respectively. The method of calculating the flux corrections is described in Section 2-3. Note that in the coupled model, flux corrections do not influence the atmospheric model at all: they are only used to bring the ocean model SST close to climatological values when the MLM is forced with atmospheric variables. The first 4 1/3 years of the simulation are not used in the analysis to allow the models to reach an equilibrium. The coupled model data is processed from the first of May of year 5 to April 30th of year 36. The initial conditions for ocean temperature, salinity, and mixed layer depth are identical to those used for the partially coupled sensitivity experiments discussed in Chapter 3.

The control (CON) simulation is integrated for 35 1/3 years, and there is no interannual variability of sea surface temperatures but there is an annual cycle. The ocean temperature climatology in the control simulation is prescribed as the long term mean of the coupled simulation in all of the ocean basins[1]. The ocean temperature climatology in the oceanic regions other than the North Atlantic is from Alexander and Mobley (1976) for both the control and coupled simulations. The first 1 1/3 years of the control simulation are not included in the analysis, leaving 31 years of model data starting from May of year 2 to April of year 32.

Long term monthly means of the model fields are calculated by averaging the 31 monthly values. Monthly anomalies are constructed by subtracting the long term mean for a given month from the monthly mean during individual model years. In the coupled simulation there was no noticeable drift in ocean temperature or mixed layer depth over the 31 year integration, and therefore the data have not been detrended. The analysis focuses primarily on the autumn and winter months, September to March.

---

1. The coupled simulation was integrated before the control, making it possible to prescribe climatological ocean temperatures in the North Atlantic that are identical to those in the coupled simulation. The control simulation discussed in this chapter is different from the CCM1 (case 256) control integration used in the work shown in Chapter 2 and 3. The long term mean SST climatology of the coupled simulation is not exactly the same as the Alexander and Mobley (1976) SST climatology in the North Atlantic.

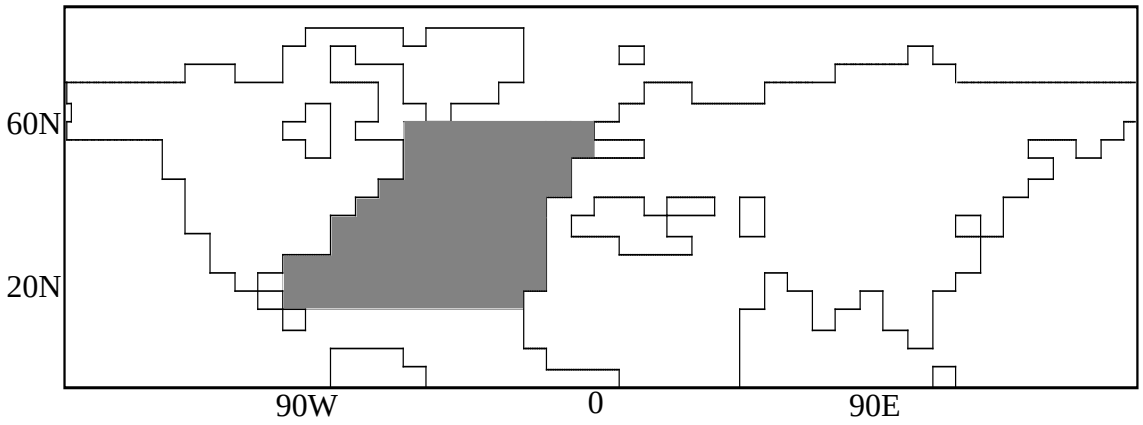

Figure 4-1. Schematic of the Northern Hemisphere in the R15 version of CCM1. Shading represents the mixed layer model (MLM) in the North Atlantic Ocean in the coupled simulation.

4.2 Climatology and Variance

4.2.1 Mean Fall and Winter Climatology

Seasonal and monthly difference maps are constructed by subtracting the long term mean of the control from the coupled simulation for each climate field. Statistical significance is assessed using the Student's t-test for significantly different means (Press et al., 1990). The discussion focuses on the fall and winter months of the year, defined as the average over September to November (SON) and December to February (DJF), respectively.

The seasonal mean wintertime (December to February) surface fluxes, precipitation, sea-level pressure, air temperature, air moisture, and winds indicate that over the North Atlantic there are few significant differences between the control and the coupled simulations. Differences significant at the 5% level are reached at 4 gridpoints in total surface heat flux (Q_{tot}) and at none in air temperature and sea-level pressure. The climatologies of the 500 mb heights of the coupled and control simulations are also not significantly different. Differences between the mean climatologies of the coupled and uncoupled simulations are larger though not more significant, when individual months are compared. Overall the

mean climatologies of the atmospheric components of coupled and control simulations are not found to be significantly different.

Mean entrainment heat flux (Q_{we}) acts to cool the mixed layer during autumn (September to November) (Figure 4-2a) and winter (December to February) (Figure 4-2b). The heat flux due to entrainment (Q_{we}) is calculated as follows:

$$Q_{we} = -w_e \cdot (T_{mix} - T_{below}) \cdot \rho_0 \cdot C_p \qquad \textbf{(4-1)}$$

where w_e is entrainment velocity, T_{below} the temperature below the mixed layer, T_{mix} the mixed layer temperature, ρ_0 the reference density of ocean water, and C_p the specific heat of water. The cooling due to entrainment is largest in the fall months when the mixed layer is deepening and entrainment values are large. Observations of entrainment over the midlatitude North Atlantic are not available for comparison. The mean entrainment heat flux is approximately 30% of the net heat flux ($Q_{net} = Q_{cor} + Q_{tot}$) during fall (SON) and 50% during winter (DJF).

Model mixed layer depth nearly doubles between SON (Figure 4-2c) and DJF (Figure 4-2d). The mixed layer depth in the model is deepest at most grid points in February. The observed maximum mixed layer depths in the midlatitude North Atlantic are between February and March based on the Levitus (1982) temperature criterion (see Table 2-1). The model mixed layer depths begin to shallow slightly earlier than the observations.

The root-mean-square of the 500mb height from November to April is a measure of the model storm track activity or more specifically synoptic scale activity since both highs and lows are included in the calculation. Details of how this quantity is calculated are given in Section 2-2. The 500 mb RMS averaged for the 31 winters from the coupled (Figure 4-3b) and the control (Figure 4-3a) simulations are nearly indistinguishable.

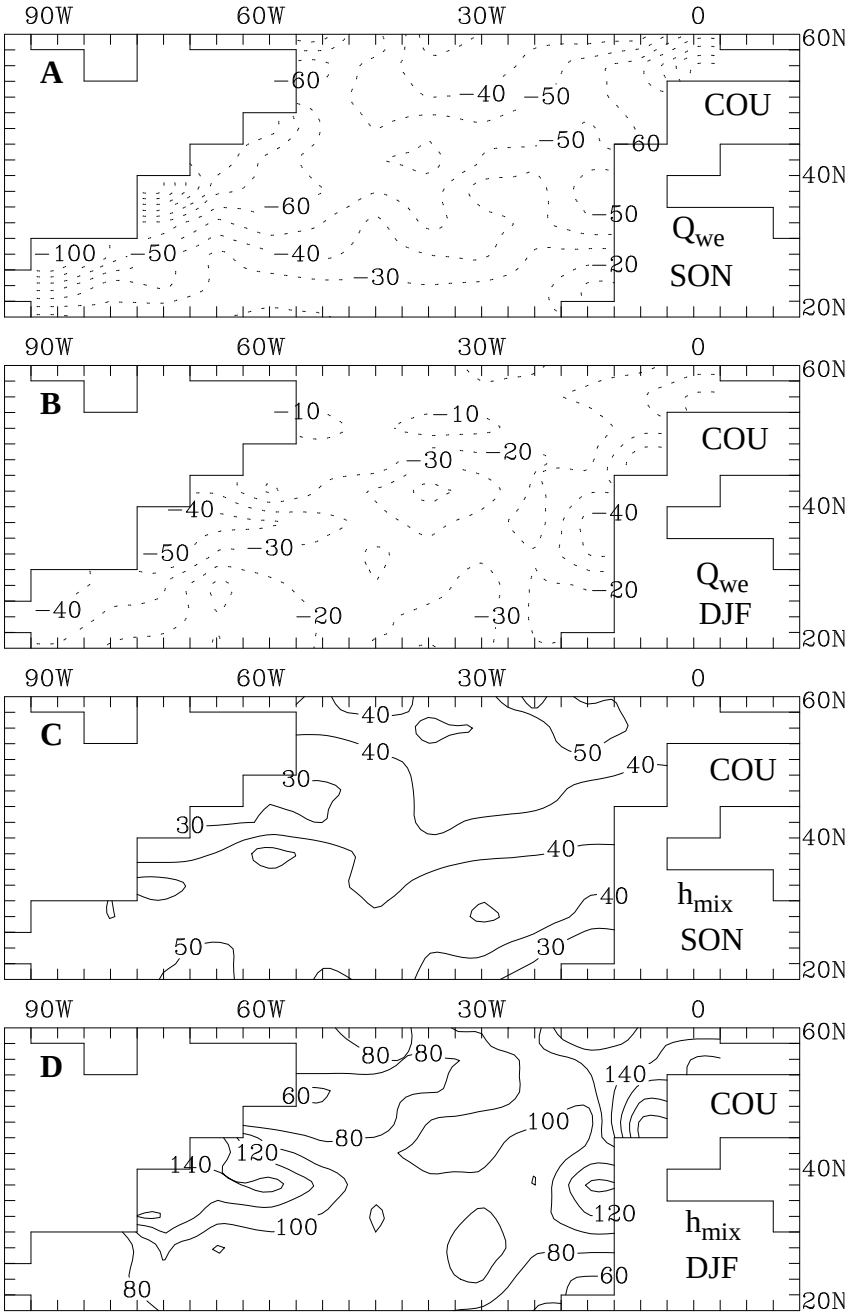

Figure 4-2. Long term climatologies for a) SON entrainment heating (Q_{we}) b) DJF Q_{we}, c) SON h_{mix}, and d) DJF h_{mix} (C. I. is 10 W m^{-2} for Q_{we} and 20 m for h_{mix}).

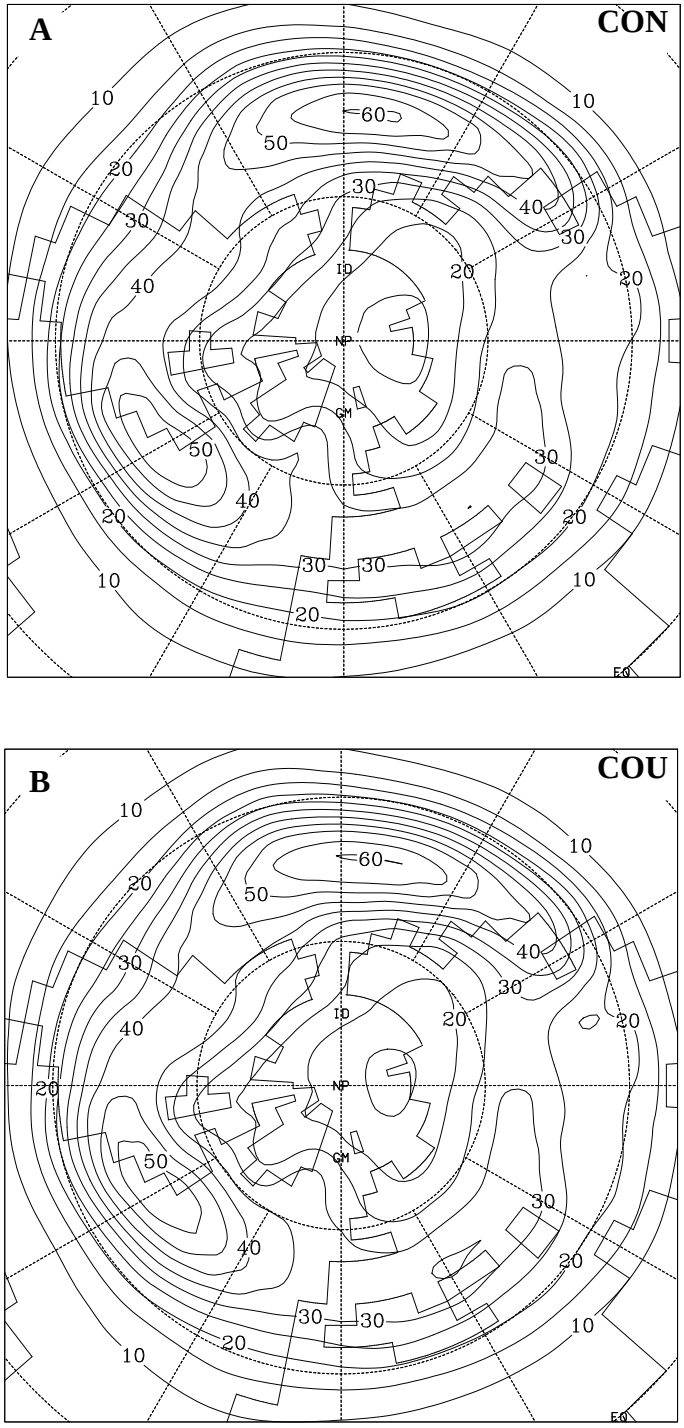

Figure 4-3. Root-mean-square of band passed daily 500 mb heights from the a) control and b) coupled simulations. Units are geopotential meters and C.I. is 5 gm.

4.2.2 Wintertime Climate Anomalies

The variance of the coupled and the control simulations is calculated from monthly and seasonally averaged anomalies. An F-test (Brooks and Carruthers, 1953) is used to assess the significance of the change in variance between the control and coupled simulations. The plots are presented as a ratio of coupled over control standard deviations. Shading indicates a significance level of 95% or greater. The analysis focuses on the variance calculated from seasonally (DJF) averaged anomalies.

Air temperature (T_{air}) variance is significantly enhanced in the coupled simulation (Figure 4-4a) during the winter season (DJF) and also for the average of November to April (not shown). The largest values (>0.6 ˚C) of standard deviation of T_{air} in the control case are found close to the coast of North America (Figure 4-4b) but in the coupled case (Figure 4-4c) the larger values extend far from the coastline to better resemble the observations (Figure 4-4d). This result suggests that an interactive ocean is important in increasing the area of high variability of air temperature (T_{air}) from just near the coast to a much larger area of the ocean, which may be explained by the following mechanism. In the control simulation, continental air moves over an ocean with no variability, and anomalies in air temperature are quickly damped. However, in the coupled simulation, continental air moves over an ocean that can respond to the atmospheric anomalies, which results in a slower damping of air temperature anomalies. Therefore, in the coupled simulation continental air with its characteristically large variability is able to move farther over the ocean before anomalies are damped.

The variance of air moisture (q_{air}) is also enhanced with coupling (Figure 4-5a) during the winter season (DJF). The standard deviation increases most in the subtropical regions with coupling (compare Figure 4-5b and Figure 4-5c). However, both the control and the coupled simulations underestimate the observed variability of air moisture (Figure 4-5d).

The variability in the total surface heat flux (Q_{tot}) decreases with coupling over the DJF season (Figure 4-6a). The significant decrease in the variance of Q_{tot} is largely due to

decreases in sensible and latent heat flux variability (not shown). Variability of the total heat flux in the control case is a maximum along the coast of North America and decreases eastward (Figure 4-6b). With an interactive ocean the variability of the total heat flux (Figure 4-6c) has decreased, particularly near the coast of North America. The observed variability is estimated using heat fluxes calculated from COADS data (Figure 4-6d) and is larger than that from the coupled simulation. The variability of observed heat fluxes is expected to be larger than that from the model. In nature, heat fluxes are influenced by advection in the ocean, a process neglected in the MLM, and storm track activity, which is weaker in the model than in observations.

The averaged DJF variance of pressure (not shown) is slightly smaller in the North Atlantic region in the coupled than the control simulation. There is also a slight, but not statistically significant, decrease over the North Atlantic sector in the variance of the 500 and 200 mb heights (not shown) for seasonal averaged variance over DJF.

The standard deviation ratios based on the individual months of December, January, and February (31*3 degrees of freedom) are also calculated. The ratios of coupled over control standard deviations for T_{air}, q_{air}, Q_{tot} and 500 mb height are much closer to 1, indicating a smaller difference between the two simulations, when the individual months are used to calculate the variances. The monthly anomalies of air temperature (moisture and heat flux) from the control simulation are of roughly the same amplitude as those in the coupled simulation. Therefore in the coupled simulation there is a larger change in the variance on seasonal than on monthly time scales.

The standard deviations of ocean surface temperature for DJF from the coupled simulation (Figure 4-7a) ocean surface temperature resembles the observed (Figure 4-7b) but is slightly weaker in magnitude. It is not surprising that the model ocean temperature variability along the coast of North America is weaker since the ocean model does not contain advective effects, and the atmospheric storm tracks are weaker than observed. The standard deviation of entrainment heat flux during fall (Figure 4-8a) and winter (Figure 4-8b) is nearly equal in size. The variability of heating due to entrainment is largest near the east

coast of North America and is located in the region of largest heat flux variability. The standard deviation of mixed layer depth during fall (Figure 4-8c) is between 4-5 meters throughout the domain. In contrast, during DJF (Figure 4-8d) the standard deviation is considerably larger near the east coast of the North America and in the far northeastern Atlantic Ocean. The area of largest mixed layer depth variability during the fall and winter is generally collocated with the areas of large entrainment heating with the exception of the large variability in the far northeastern Atlantic Ocean. In the northeastern Atlantic Ocean the mean surface heat fluxes act to strongly cool the surface, and the winter temperatures are weakly stratified, resulting in large mixed-layer depths.

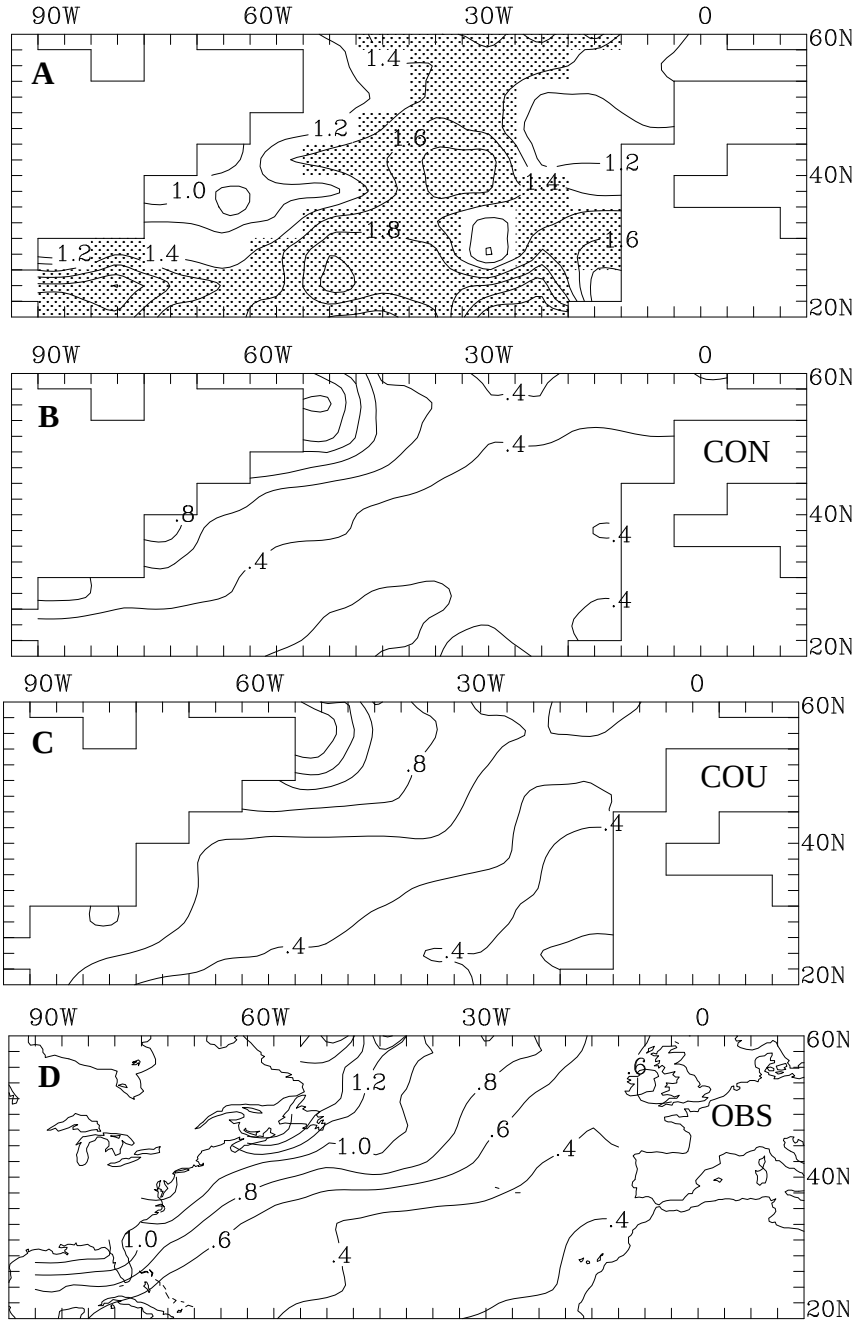

Figure 4-4. DJF values of a) ratio of coupled over control T_{air} standard deviation, and standard deviations of T_{air} from the b) control, c) coupled, and d) COADS observations. Units are ˚C and contour intervals are 0.2 in panel a. C.I. is 0.2 ˚C in panels b-d. Shading indicates significance at the 95% or greater level using an F-test.

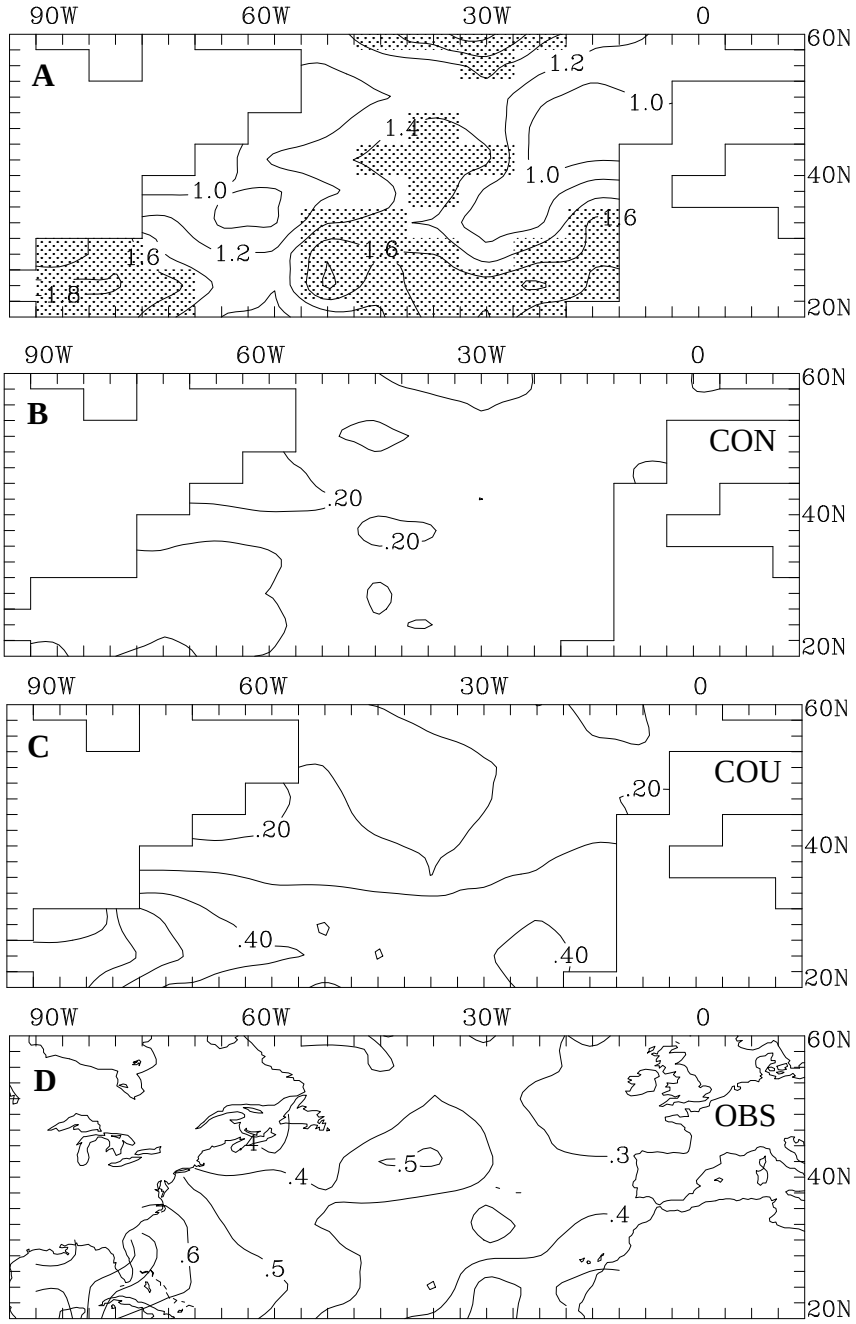

Figure 4-5. DJF values of a) ratio of coupled over control q_{air} standard deviation, and standard deviations of q_{air} from the b) control, c) coupled, and d) COADS observations. Units are g kg^{-1} and contour intervals are 0.2 in panel a. C. I. is 0.1 g kg^{-1} in panels b-d. Shading indicates significance at the 95% or greater level using an F-test.

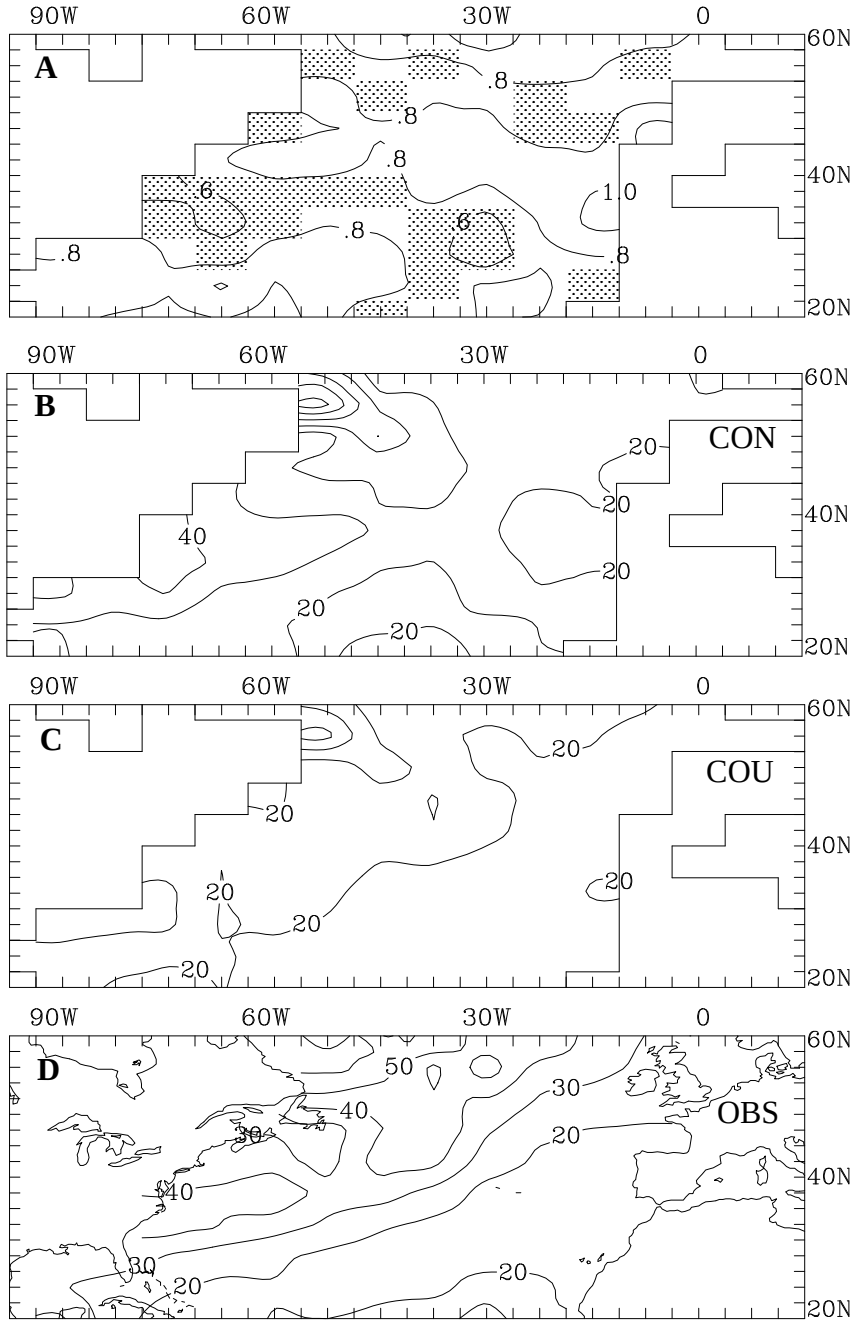

Figure 4-6. DJF values of a) ratio of coupled over control Q_{tot} standard deviation, and standard deviations of Q_{tot} from the b) control, c) coupled, and d) COADS observations. Units are W m^{-2} and contour intervals are 0.2 in panel a and 10 W m^{-2} in b-d. Shading indicates significance at the 95% or greater level using an F-test.

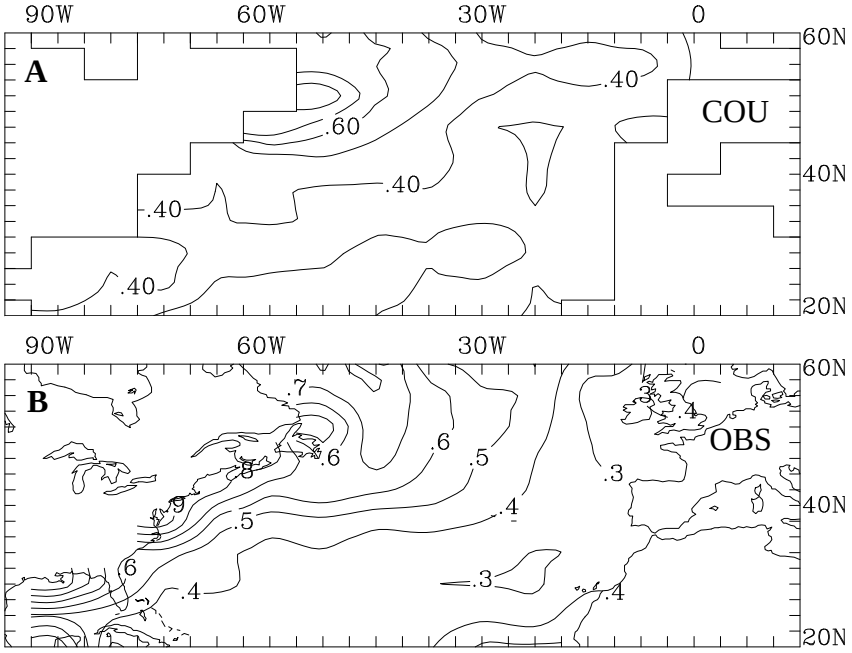

Figure 4-7. Standard deviation of ocean surface temperature for a) coupled simulation and b) COADS observations for averaged anomalies over November-January. Units are in ˚C and the C.I. is 0.2˚C.

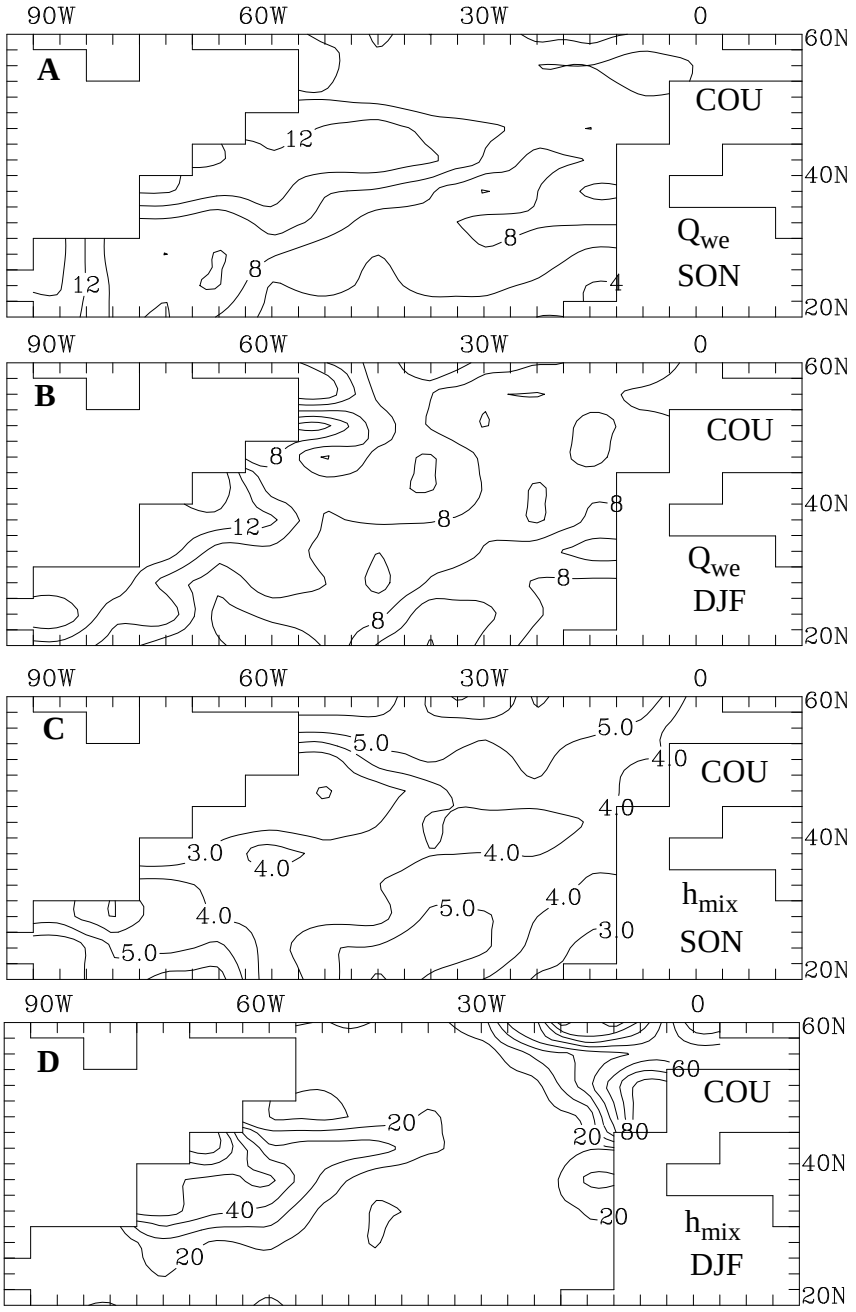

Figure 4-8. Standard deviation using 3 month average anomalies a) SON Q_{we} b) DJF Q_{we}, c) SON h_{mix}, and d) DJF h_{mix}. Units are W m^{-2} in panel a and b. Units are in meters in panels c and d.

4.3 Relationships Between Air-Sea Variables

Linear correlation coefficients are calculated between seasonally (DJF) averaged anomalies of air temperature and total heat flux. Significance is assessed using Student's t-test, and the reduction of the total degrees of freedom due to persistence is calculated according to the methods of Quenouille (1959). The majority of gridpoints contain correlations coefficients larger than approximately 0.3 which are significant at the 95% or greater level. Shading has been omitted to simplify viewing of these correlation plots.

Correlations between air temperature (T_{air}) and total heat flux (Q_{tot}) for seasonally averaged DJF anomalies are approximately 0.9 in the control case (Figure 4-9a) and 0.6 in the coupled run (Figure 4-9b). The observed correlations between T_{air} and Q_{tot} (Figure 4-9c) are characterized by stronger (weaker) correlations in the northwest (southeast) part of the domain. The coupled result is similar to the observations (Figure 4-9b).

Correlations are also calculated between T_{air} and Q_{tot} using monthly anomalies from December to February (31*3 = 93 degrees of freedom) for the control, coupled, and observed data. The control case correlations (not shown) based on individual winter months resemble the control seasonal correlations (Figure 4-9a). However, the coupled and observed monthly correlations (not shown) are somewhat larger than the seasonal correlations (Figure 4-9b and c). The impact of coupling is responsible for the decrease of correlations between air temperature and heat flux with coupling.

To examine this point further, correlations between T_{mix} and Q_{tot} using the seasonal and monthly anomalies are calculated for the coupled simulation. Correlations between ocean temperature and heat flux, based on seasonal averages (not shown) are larger than those based on monthly anomalies, which is opposite the relationship found above between air temperature and heat flux. The correlations between air temperature and heat flux are smaller with coupling, most likely because on seasonal time scales part of the variance of heat fluxes is now associated with ocean temperatures. The caveat is, of course, that air and ocean temperatures vary together.

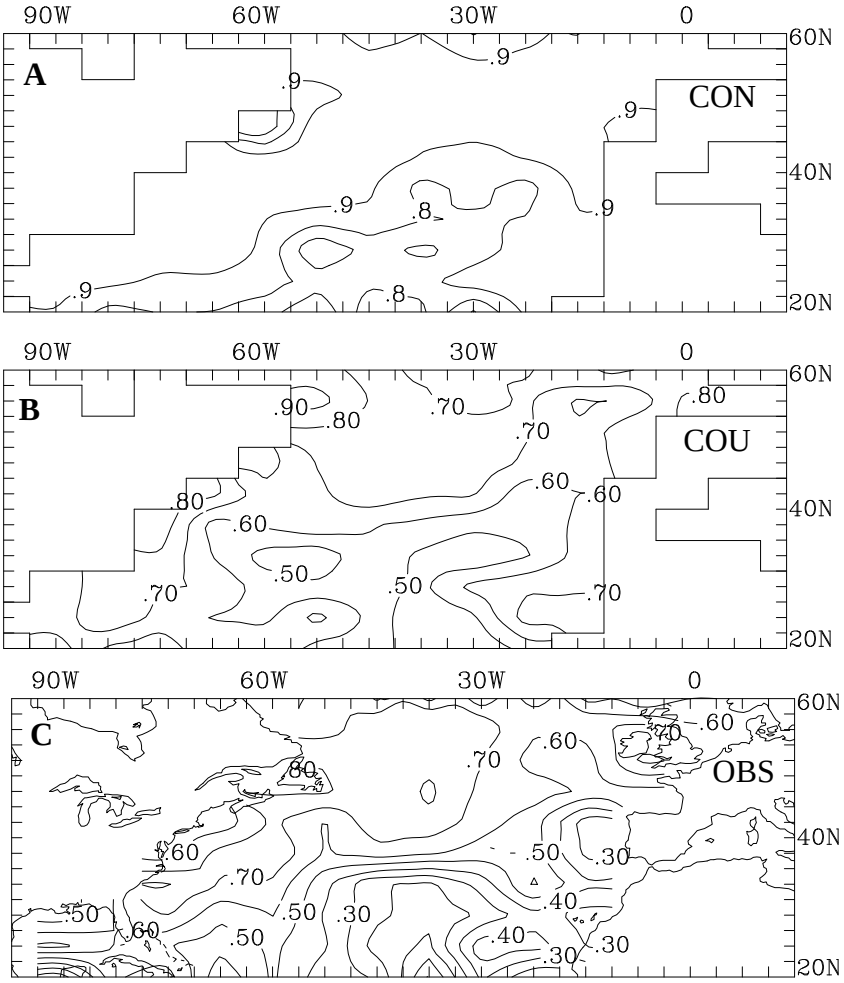

Figure 4-9. Correlations between seasonal DJF anomalies in T_{air} and Q_{tot} for a) control case, b) coupled case, and c) observations (COADS).

4.4 Natural Variability of the Model Climate

The first EOF of air temperature in the CCM1 control simulation is characterized by a north-south oriented dipole pattern and is similar to the dipole mode found in the observations. An EOF and composite analysis presented in this section examines the influence of air-sea interaction on the first EOF (dipole mode of variability).

4.4.1 Dipole Mode of Variability

Empirical Orthogonal Functions (EOF) are constructed from seasonally averaged anomalies of DJF air temperature for the control, coupled, and observed data. Because air temperature data is available for both the control and the coupled simulations, it has been chosen as the primary variable for this analysis. Air moisture, total heat flux, surface pressure, precipitation and 500mb heights are regressed onto the time coefficients of EOF1 air temperature to examine the concurrent patterns in these variables associated with the dipole mode of variability. The regression coefficients are scaled to correspond to a 1.0˚C change at the center of the northern lobe of the dipole.

The first EOF for air temperature during the months of December to February for the coupled, control, and observed data clearly displays the dipole pattern (Figure 4-10). The EOF's in Figure 4-10 are displayed in the form of correlations between the time coefficients and the total anomalies to highlight the amount of variance explained at each gridpoint by the dipole mode. The predominant mode of variability in the models (Figure 4-10 a and b) strongly resembles the observed (Figure 4-10c) and is characterized by a north-south oriented dipole with centers in the western part of the midlatitude Atlantic. The model simulations also capture the weaker positive (north) and negative (south) patterns in the eastern part of the Atlantic that are also evident in the observations. The first mode explains 27% of the total variance in the coupled case, 43% in the control case, and 30% in the observed. The total variance (numbers not shown) for the dipole mode in the coupled (control) case is approximately 56% (30%) of the observed. The correlations in the southern part of the dipole are weaker by approximately 50% in the coupled simulation than the control case.

The time coefficients for the first EOF of T_{air} for the coupled, control, and observed data are presented in Figure 4-11. There is a tendency in the time coefficients of observed air temperature (Figure 4-11c) of the dipole mode to vary at frequencies near decadal as well as biennial time scales (Deser and Blackmon, 1993). With the inclusion of an interac-

tive ocean the variability of the time coefficients of air temperature of the dipole mode (Figure 4-11b) contains more lower frequency variability than the control.

Regression coefficients of air moisture, total heat flux, surface pressure, and precipitation (Figure 4-12) on the time coefficients of EOF1 of T_{air} for the coupled simulation are consistent with the patterns of EOF1 and the observed composites examined in Chapter 3. Anomalously cool air is associated with reduced moisture, increased heat flux by the ocean, and low surface pressure to the north of the cool air. Regression coefficients for air moisture, total heat flux, surface pressure, and precipitation (Figure 4-13) on the time coefficients of EOF1 of T_{air} for the control simulation display patterns very similar to those of the coupled but with different magnitudes. The change in air moisture associated in 1.0˚C change of the time coefficient is nearly 60% larger in the southern part of the control than in the coupled simulation. Changes in heat flux and pressure associated with a 1.0˚C change of the time coefficient are also larger in the control simulation. The precipitation patterns in the coupled (Figure 4-12d) and control (Figure 4-13d) simulations are of opposite sign in the southern part of the domain. The maximum regressions are farther off shore for air moisture and total heat flux in the coupled simulation than the control simulation. This would be consistent with increased variance of air temperature seen farther off shore in the coupled compared to the control (see Figure 4-4b and c) simulation. It is likely that air-sea interaction acts to extend the anomalies locally and atmospheric advection moves them farther east before they are damped.

Regressions of 500 mb height (Figure 4-15) on the time coefficients of the first EOF of air temperature reveal differences in the patterns over Europe. Downstream of a cold northern dipole there is a positive height anomaly in the 500 mb heights (Figure 4-15b) in the coupled simulation. This feature is not as localized in the control simulation, where the regression patterns in 500 mb height (Figure 4-15a) broader and weaker. This difference over Europe between the coupled and control simulations is not as evident in regressions of surface pressure on the time coefficients of EOF1 of air temperature (Figure 4-14). The positive height anomalies associated with anomalously cold air in the North Atlantic is a

feature found in GCM simulations where the SST anomalies are specified (Palmer and Sun, 1985 and others). In addition, this positive height anomaly pattern over Europe associated with the dipole mode of variability has been identified in observations using singular value decomposition (SVD) analysis between ocean temperature and 500 mb heights in the North Atlantic (Wallace et al., 1992; Deser, personal communication).

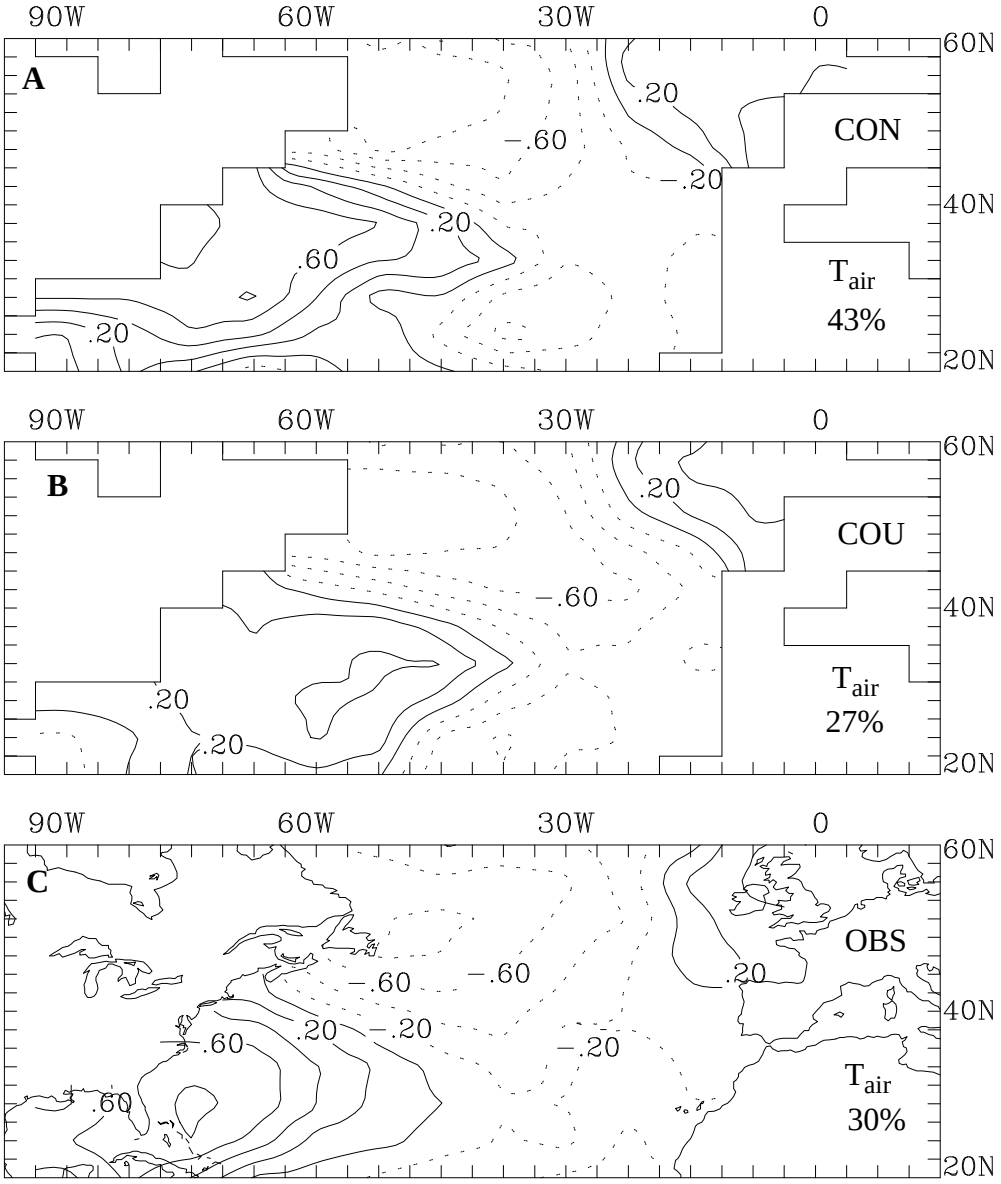

Figure 4-10. EOF 1 of air temperature for a) control simulation, b) coupled simulation, and c) observations (COADS) for seasonal wintertime (December-February) anomalies. The maps are presented as a correlation between the time coefficient of EOF1 and the full air temperature data.

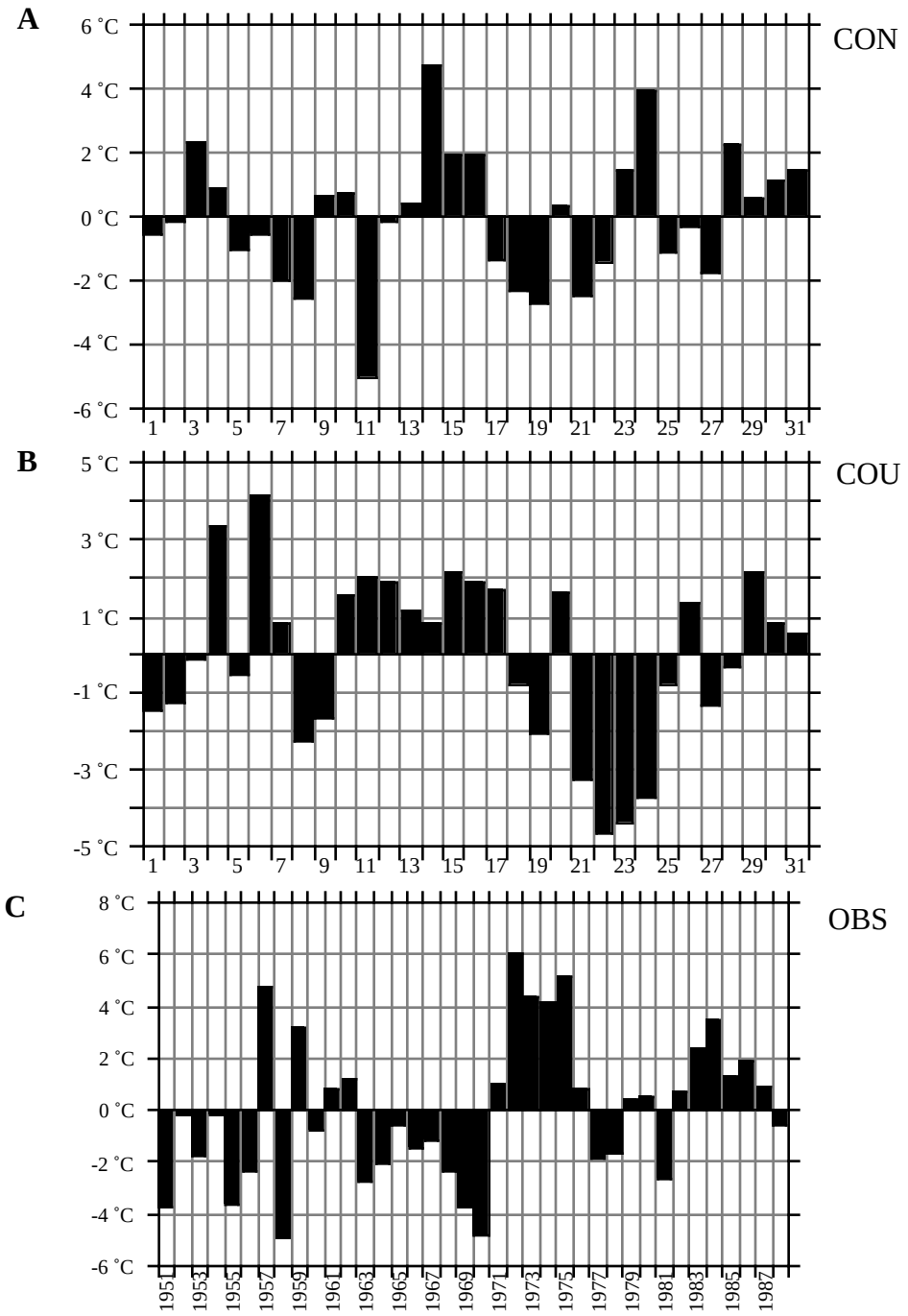

Figure 4-11. Time coefficients for EOF1 of T_{air} for a) control, b) coupled, and c) observations (COADS) for seasonal wintertime (DJF) anomalies. The units are ˚C. The year label on the x-axis refers to January and February.

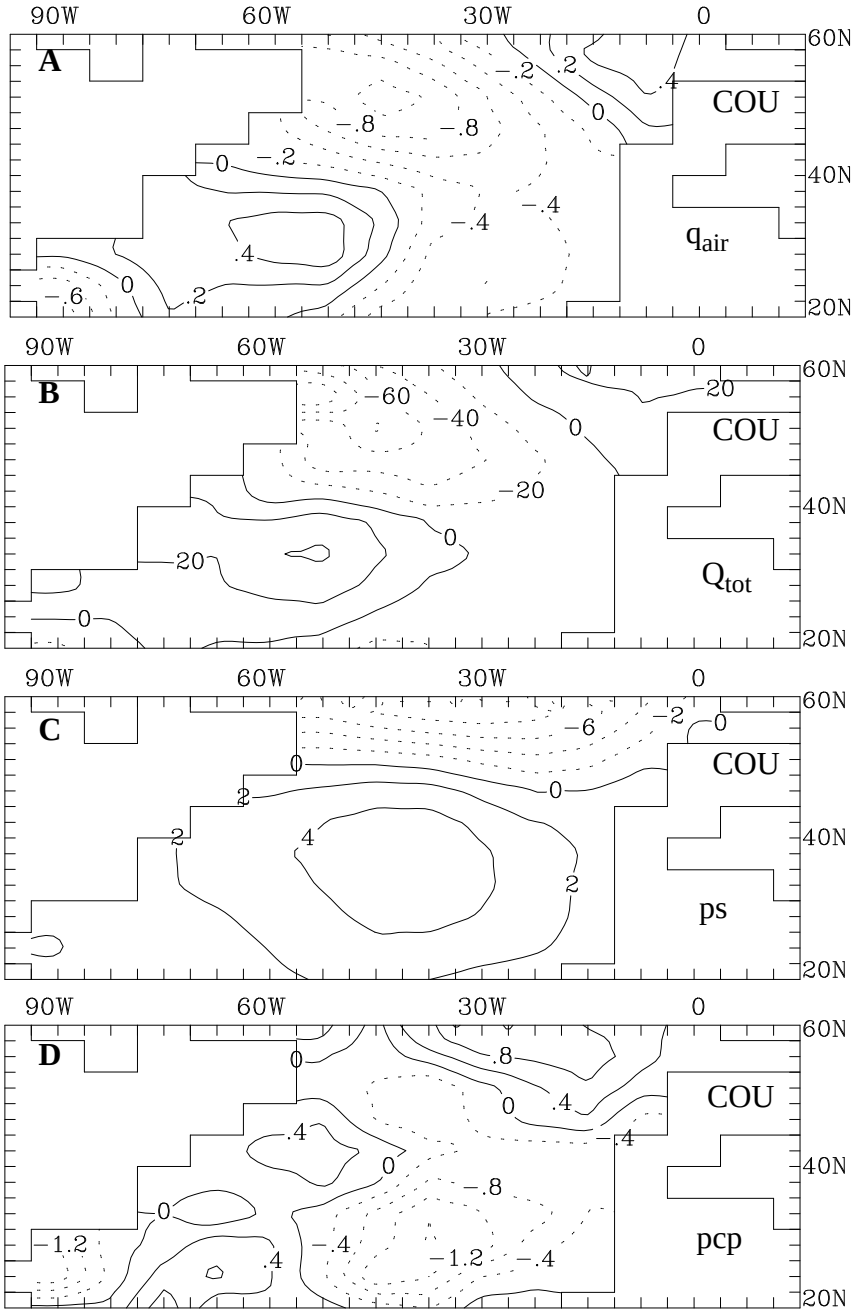

Figure 4-12. Regressions from the coupled simulation during wintertime (DJF) of various atmospheric fields on the time coefficients of EOF1 of T_{air}. The fields are a) q_{air} (units of g kg^{-1} per 1˚C), b) Q_{tot} (W m^{-2} per 1˚C), c) surface pressure (ps) (mb per 1˚C), and d) precipitation (pcp) (mm day^{-1} per 1˚C).

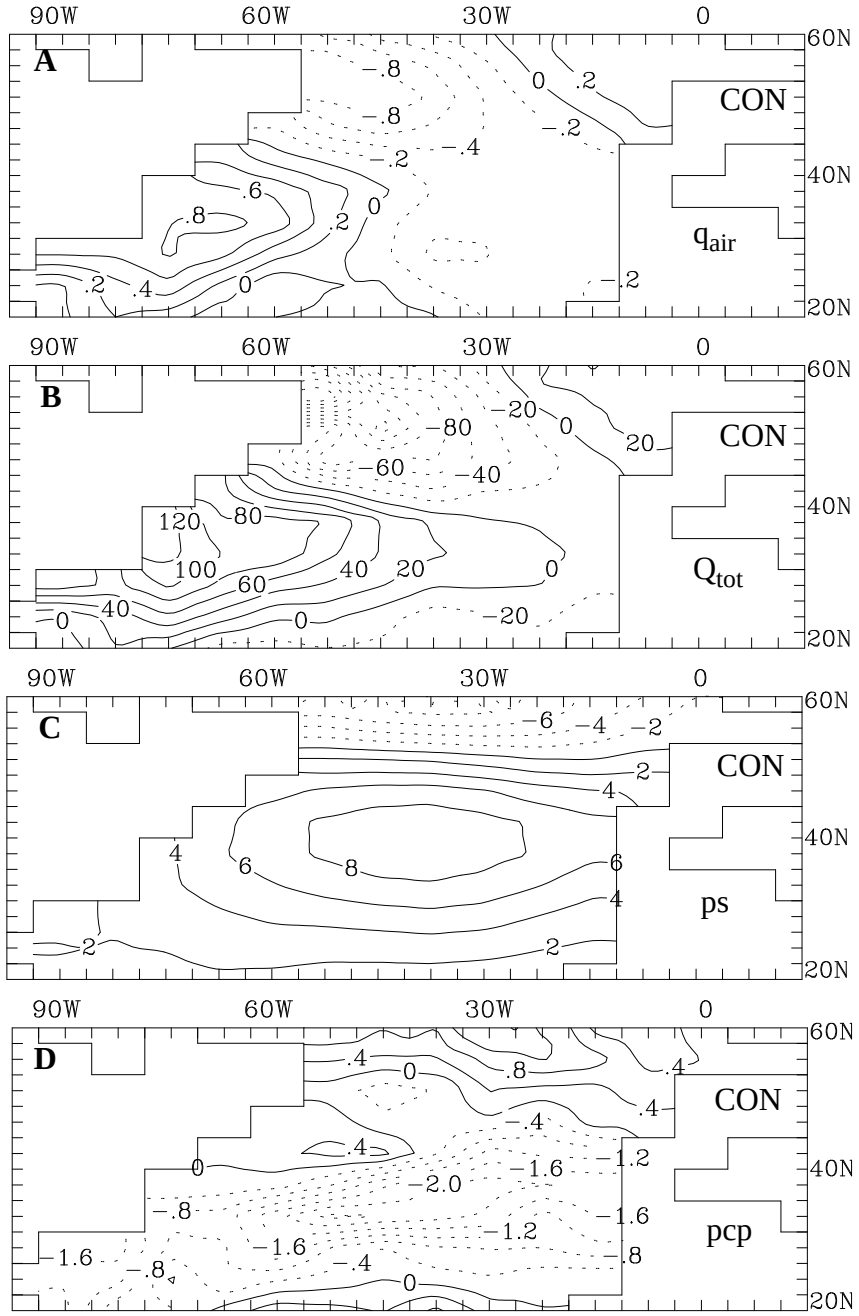

Figure 4-13. Regressions from the control simulation during wintertime (DJF) of various atmospheric fields on the time coefficients of EOF1 of T_{air}. The fields are A) q_{air} (units of g kg^{-1} per 1˚C), B) Q_{tot} (W m^{-2} per 1˚C), C) surface pressure (ps) (mb per 1˚C), and D) precipitation (pcp) (mm day^{-1} per 1˚C).

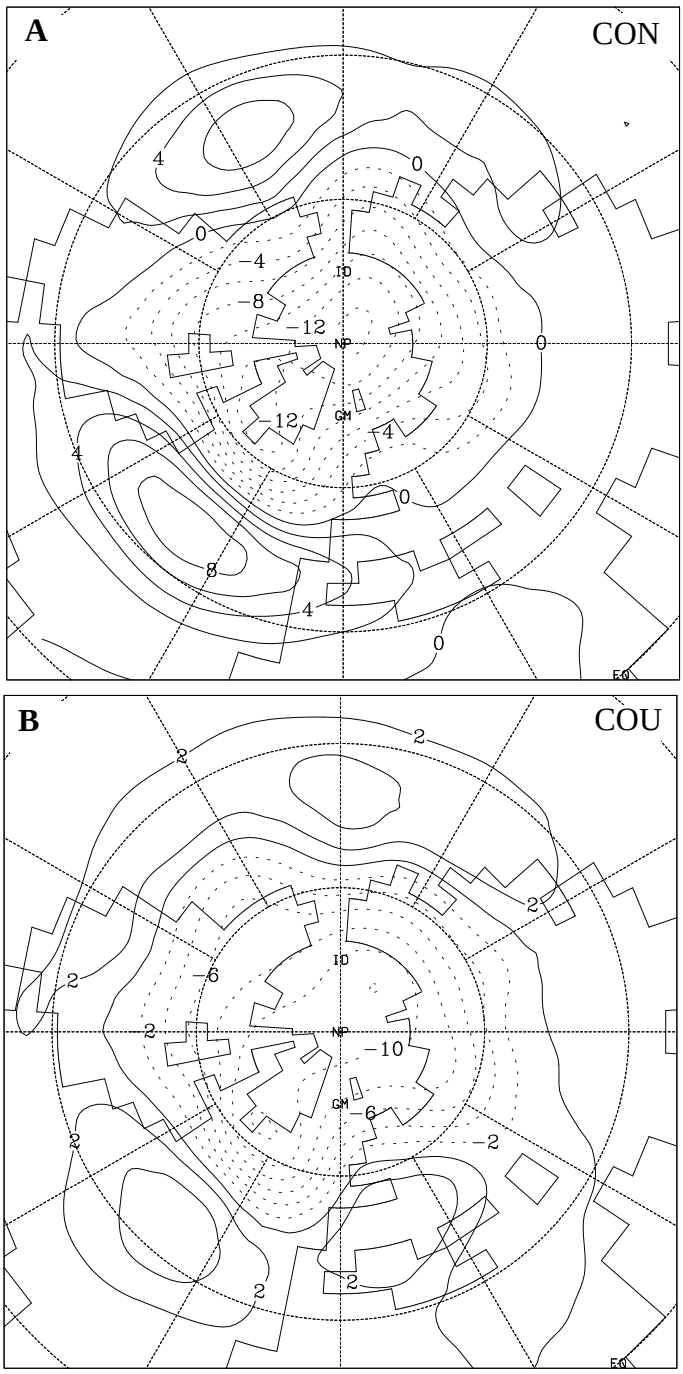

Figure 4-14. Regressions during wintertime (DJF) of a) control surface pressure and b) coupled surface pressure on their respective time coefficients of EOF1 of T_{air}. Units are mb per 1˚C.

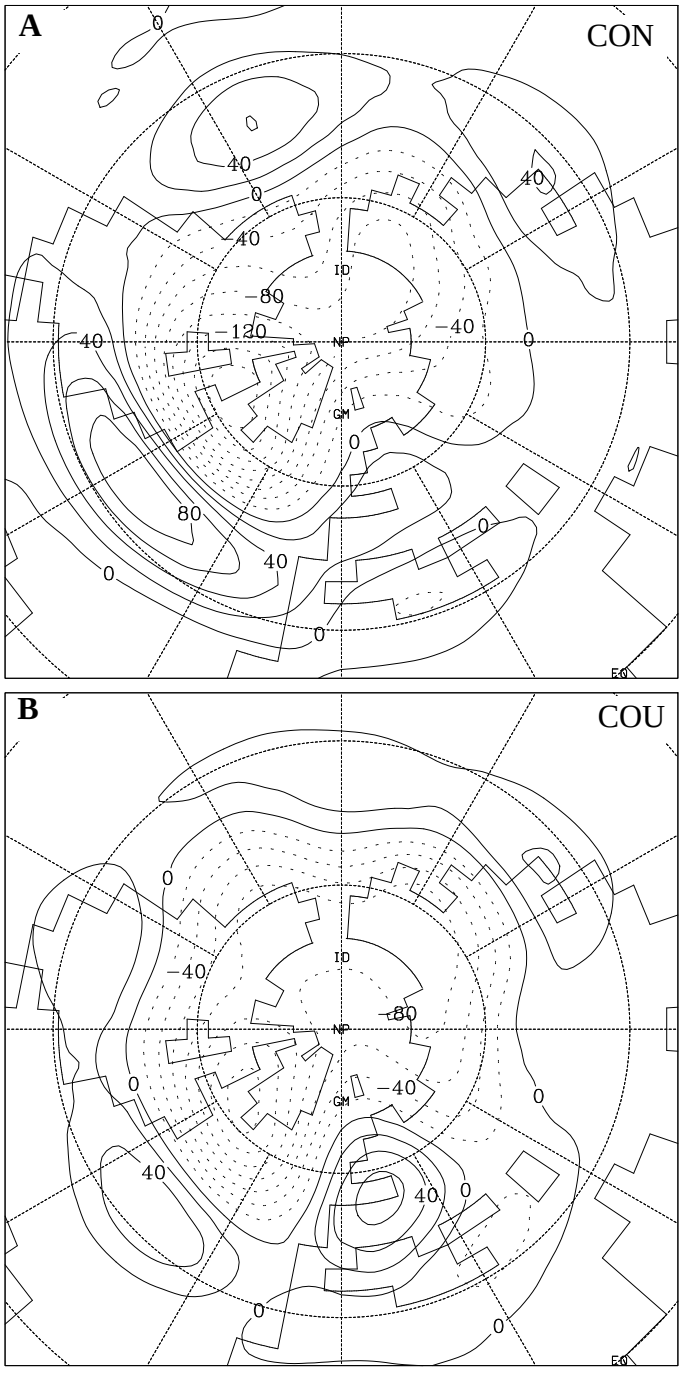

Figure 4-15. Regressions during wintertime (DJF) of a) control 500 mb height and b) coupled 500mb height on their respective time coefficients of EOF1 of T_{air}. Units are gm per 1˚C.

4.4.2 WARM and COLD Epochs of Dipole Variability

The anomalies are presented in composite form to confirm the EOF results as well as to compare and contrast the magnitudes of the control and coupled anomalies associated with the dipole mode of variability. A seasonal (DJF) examination is found in Section 4.4.2.1. A benefit of composites is that they allow nonlinearities between warm and cold phases of the pattern to be visible.

The eight WARM and COLD cases, defined by the sign of the anomaly in the northern half of the domain, are listed in Table 4-1. These were selected based on the time coefficients of EOF1 of air temperature for seasonally averaged anomalies DJF (Figure 4-11): years when the time coefficient is larger than half the standard deviation are eligible to comprise the WARM and COLD averages. In addition the sign of the time coefficients of EOF1 of air temperature for the seasonally averaged November to March must be of the same sign, to ensure that the anomaly was reasonably long lived. It was decided to use the same number of total winter seasons for each composite and that turned out to be eight, which was the maximum of the cold coupled cases. The strongest eight winters that met the two criteria were chosen to comprise the warm coupled case. There were 11 cold and eight warm winters that satisfied the requirements in the control case. The three cold winters with the smallest time coefficients were eliminated from the control cold composites. The eight winters that comprise the WARM and COLD cases are listed in Table 4-1.

COU Warm	COU Cold	CON Warm	CON Cold
2	4	7	3
8	6	8	14
19	11	11	15
21	12	18	16
22	15	19	23
23	17	21	24
24	20	25	28
27	29	27	30

Table 4-1. List of winter seasons that comprise the warm and cold composites for the coupled and control warm and cold cases (sign of anomaly in the north).

4.4.2.1 Analysis of Winter Months (DJF)

The warm composites for air temperature and heat flux are displayed in Figure 4-16 for the coupled and control simulations. The anomalies are larger for heat flux in the control simulation whereas the temperature anomalies are slightly larger in the northern half of the domain in the coupled simulation than in the control simulation.

The mixed-layer ocean temperature anomalies (Figure 4-17a) are slightly smaller than air temperature anomalies (Figure 4-16a) in the coupled simulation, suggesting the circulation features force mixed layer temperature anomales and not vice versa. Mixed layer depths (Figure 4-17b) are anomalously shallow (deep) in the region of warm (cold) ocean temperatures. Anomalous heating due to entrainment in the fall months (Figure 4-17c) acts to enhance the dipole anomaly whereas during the winter (Figure 4-17d) it acts to damp the temperature anomaly in the north half of the basin.

Air temperature for the cold coupled (Figure 4-18a) and control (Figure 4-18c) composites are nearly equal in magnitude in both the southern and the northern part of the domain. Total heat flux anomalies are nearly 40% larger in the control (Figure 4-18d) than the

coupled (Figure 4-18b) cold composite.

The mixed-layer ocean temperature anomalies (Figure 4-19a) are slightly smaller than air temperature anomalies (Figure 4-18a) in the coupled simulation for the cold composites. Similar to the warm composites, circulation features are those associated with the atmosphere forcing the ocean and not vice versa. Mixed layer depths (Figure 4-19b) are anomalously shallow (deep) in the region of warm (cold) ocean temperatures in the southern (northern) part of the ocean domain. Anomalous heating due to entrainment in the northern part of the dipole acts during the fall months (Figure 4-19c) to enhance whereas during the winter (Figure 4-19d) it acts to damp the temperature anomalies.

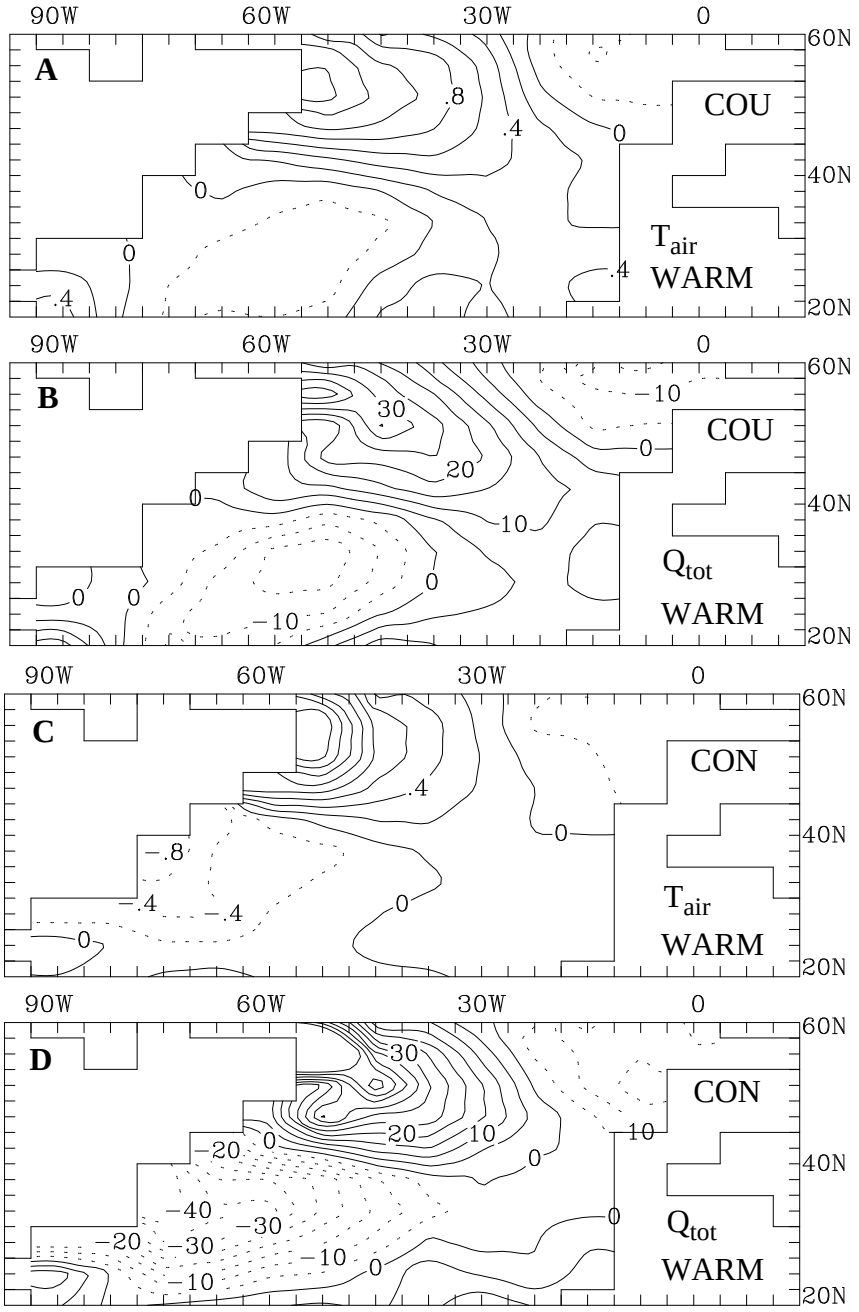

Figure 4-16. Warm composites of anomalies averaged over winter (DJF) for a) coupled T_{air} b) coupled Q_{tot}, c) control T_{air}, and d) control Q_{tot}. Units are ˚C (panels a and c) and W m^{-2} (panels b and d).

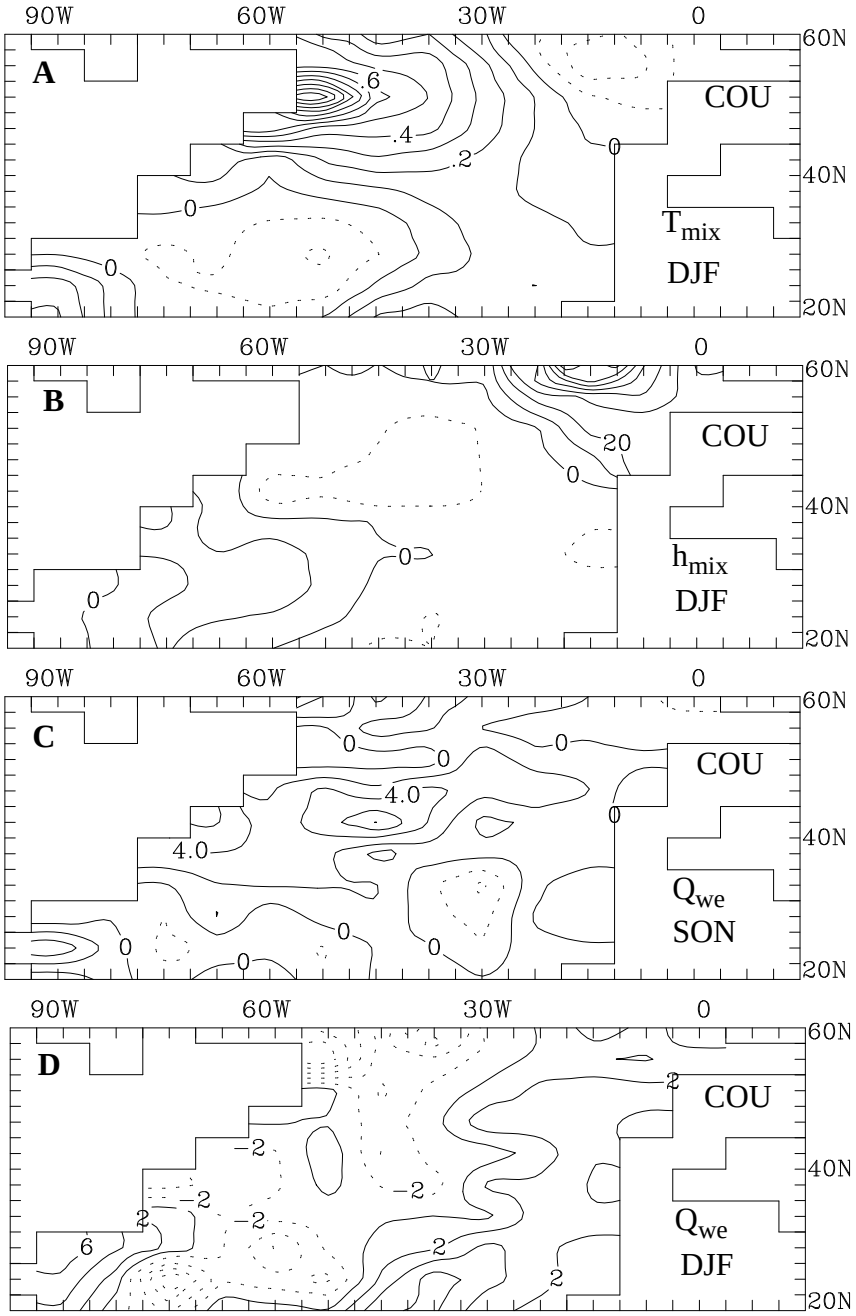

Figure 4-17. Warm composites of winter (DJF) and fall (SON) anomalies for a) DJF T_{mix}, b) DJF h_{mix}, c) SON Q_{we}, and d) DJF Q_{we}. Units are ˚C (panel a), m (panel b), and W m^{-2} (panels c and d).

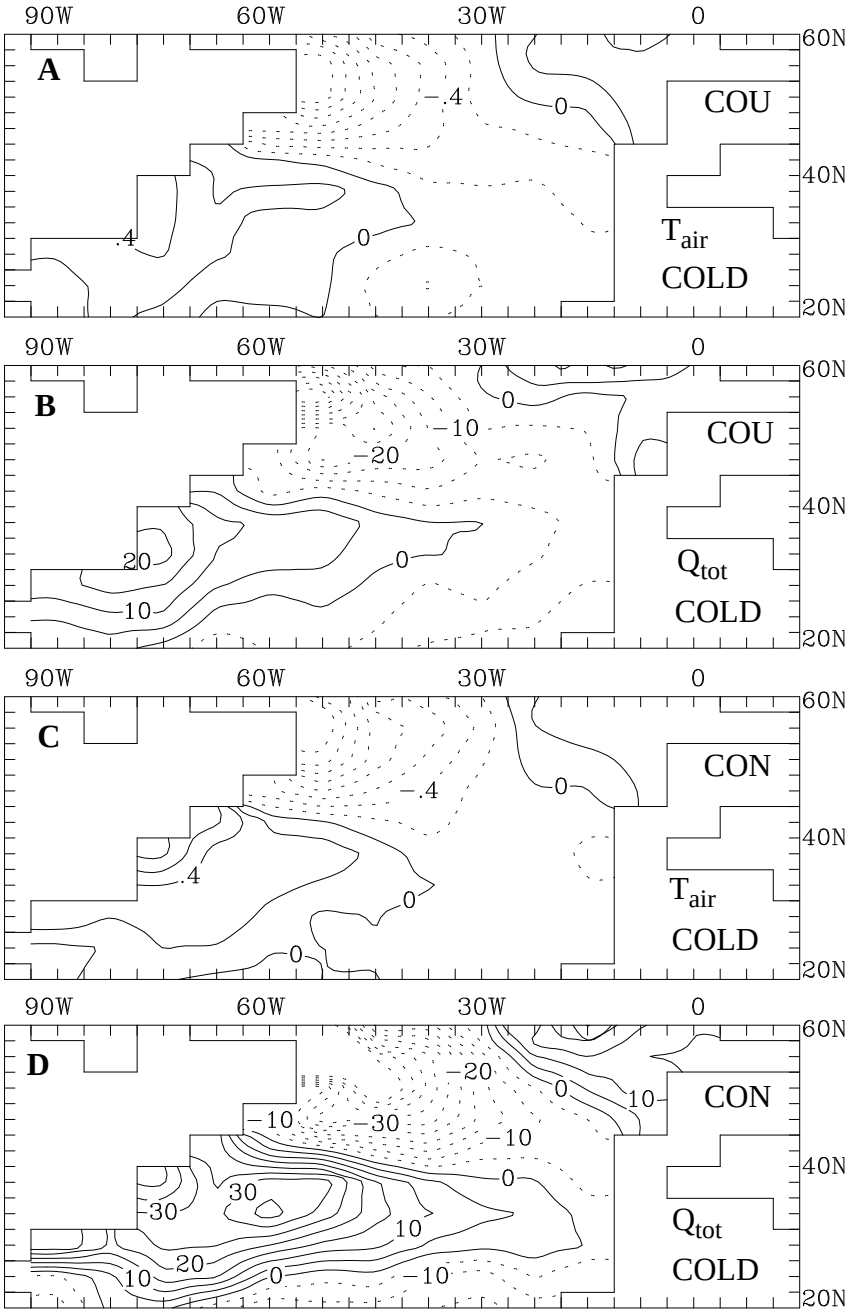

Figure 4-18. Cold composites of anomalies averaged over winter (DJF) for a) coupled T_{air} b) coupled Q_{tot}, c) control T_{air}, and d) control Q_{tot}. Units are ˚C (panels a and c) and W m^{-2} (panels b and d).

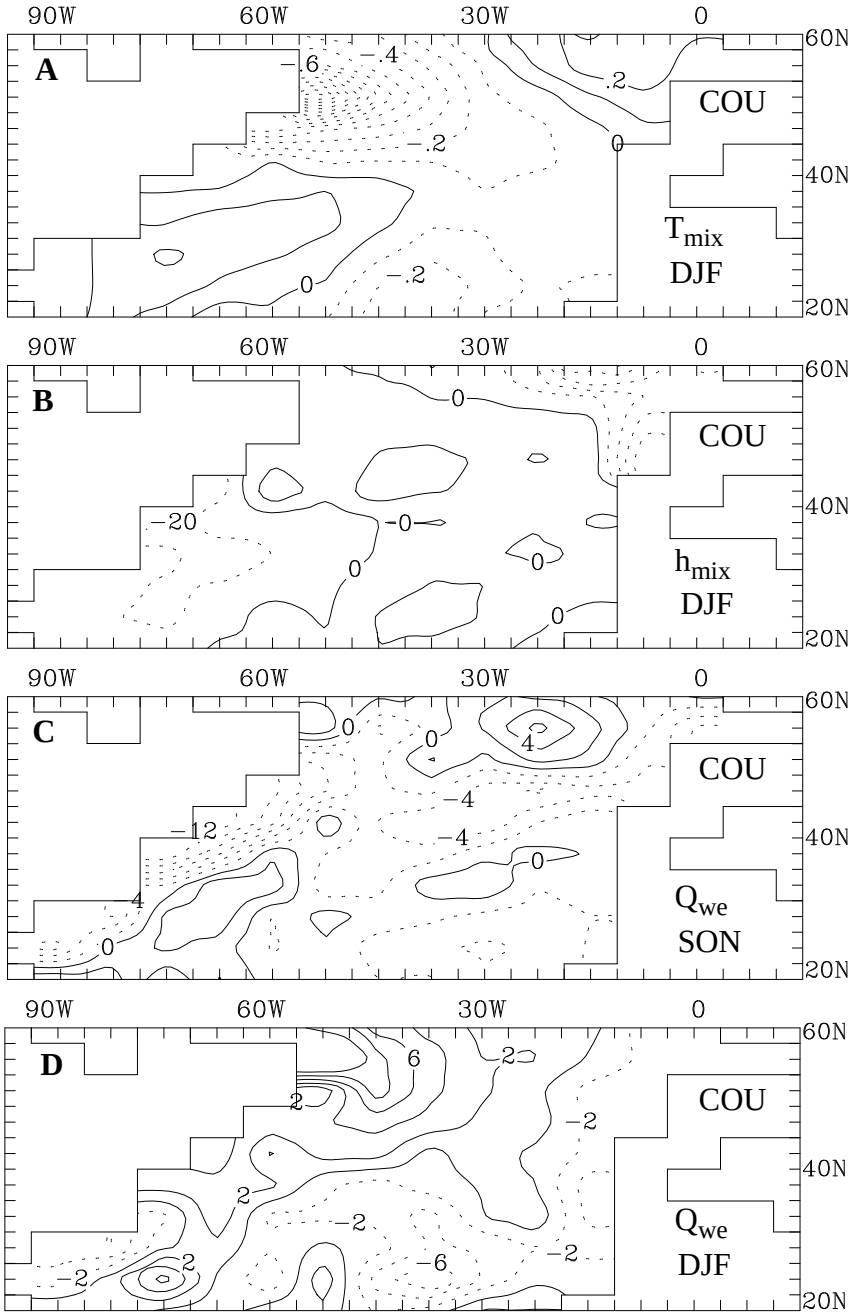

Figure 4-19. Cold composites of winter (DJF) and fall (SON) anomalies for a) DJF T_{mix}, b) DJF h_{mix}, c) SON Q_{we}, and d) DJF Q_{we}. Units are ˚C (panel a), m (panel b), and W m^{-2} (panel c and d).

4.5 Discussion

Two 31 year atmospheric general circulation model simulations using the same long term mean ocean climatology, one coupled to a variable depth mixed layer ocean in the North Atlantic and the other not, are compared to examine the role of the atmosphere-ocean interaction on interannual variability. The results presented in this chapter indicate that there are notable changes in the model climate due to the inclusion of air-sea interaction in the North Atlantic.

Seasonal air temperature and moisture variance is enhanced (Figure 4-4a) with coupling, and seasonal heat flux variance has decreased (Figure 4-6a). A plausible explanation for these changes in variance resulting from air-sea interaction, afforded by Barsugli (1995), is the following. In the control simulation, positive air temperature anomalies over fixed ocean temperatures lead to negative heat flux anomalies (out of the ocean) that act as strong negative feedback to damp the air temperature anomalies. In the coupled simulation, a positive air temperature anomaly results in reduced heat flux out of the ocean and positive ocean temperature anomalies. Since the ocean has responded to the atmospheric anomaly and the air-sea temperature difference has been reduced, the subsequent heat flux anomaly will be smaller than in the control case resulting in a weaker damping of the air temperature anomaly.

A visual inspection of the time coefficients of the EOF1 of air temperature (Figure 4-11) suggest that the dipole mode of variability is more persistent from one year to the next in the coupled simulation than the control. The changes in variance also suggest an increase in persistence of anomalies with coupling, but on a shorter time scale. An further examination of persistence is presented in Chapter 5.

This coupled simulation provides an opportunity to examine the dipole mode of variability in the ocean in terms of the surface heat fluxes and the subsurface heating due to entrainment. The latent and sensible heat flux anomalies dominate the heat budget of the dipole mode of variability both in the north and the south, in agreement with previous studies (Cayan, 1992a). Radiation flux anomalies play a negligible role in the formation of the

dipole anomalies in the ocean. Entrainment fluxes act to enhance the wintertime ocean temperature anomaly during fall and early winter in both the north and the south (not shown). However, during wintertime, entrainment acts to damp the ocean temperature anomalies in the north and continues to enhance the anomalies in the south.

4.6 Summary

A 31 year integration of CCM1 coupled to a variable depth mixed layer model (MLM) in the midlatitude North Atlantic is compared and contrasted to a 31 year control integrations of CCM1 with specified annual cycle of climatological SSTs. It is shown that air-sea interaction in the North Atlantic notably changes the climate variability.

The long term means for the winter (DJF) season for the coupled and control simulations are not statistically different for surface air temperature, surface air moisture, sea-level pressure, surface winds, total surface heat flux, 500 mb height, and 500 mb height RMS. The variances are however quite different. Coupling has increased the variance of air temperature and air moisture and reduced the variance of surface heat flux and pressure. Variability of 500 mb and 200mb heights have not significantly changed with coupling.

Compositing techniques confirm the results of the EOF analysis. The strength of anomalies in the warm and cold events are nearly equal, suggesting that the dipole mode of variability in the model is primarily linear. However, entrainment is sensitive to the sign of the oceanic anomaly. A monthly analysis of the cold event indicates that anomalous entrainment heating acts to enhance winter mixed layer temperature anomalies during the fall and damp in the winter. It is not possible to generalize for the warm event.

There are some suggestions in the analysis presented in this chapter that anomalies of air temperature persist longer in the coupled simulation. The increase in the persistence of anomalies will be examined further in the next chapter.